

# **ScienceDirect**



IFAC PapersOnLine 55-27 (2022) 299-304

# Optimal Power Analysis of a Wave Energy Converter with a Controllable Power Takeoff based on Active Motion Rectification

Lisheng Yang, Jianuo Huang, Jia Mi\*, Muhammad Hajj\*\*, Giorgio Bacelli\*\*\*, Lei Zuo\*

\*Mechanical Engineering, Virginia Tech, Blacksburg, VA 24061 USA
E-mail: {lishengyang, jianuo29, jiami, leizuo }@ vt.edu

\*\*Civil, Environmental and Ocean Engineering, Stevens Institute of Technology, Hoboken, NJ 07030 USA
E-mail: mhajj@stevens.edu

\*\*\*Sandia National Laboratories, Albuquerque, NM 87185 USA
E-mail: gbacell@sandia.gov

Abstract: This paper investigates the power generation performance of a power takeoff (PTO) system based on a newly developed active mechanical motion rectifier (AMMR), which is controllable and allows unidirectional generator rotation. The model of the PTO with a wave energy converter (WEC) is presented. A control scheme for the AMMR PTO is proposed for regular wave excitations and a semi-analytical method is developed to optimize the control parameters for maximizing generated power. The results show that more power is achieved by the AMMR PTO than a conventional PTO across a wide excitation spectrum. And the optimal control brings the motion of the WEC in phase with the excitation force.

Copyright © 2022 The Authors. This is an open access article under the CC BY-NC-ND license (https://creativecommons.org/licenses/by-nc-nd/4.0/)

Keywords: wave energy converter (WEC), power takeoff (PTO), mechanical motion rectification (MMR)

#### 1. INTRODUCTION

Ocean waves contain colossal renewable energy which serves as a critical resource towards a carbon neutral society. The energy density of ocean waves is much higher than other renewable energy resources like wind and solar (Lehmann et al., 2017). Ideally, this high energy density can lead to ocean wave power plants with compact layouts, minimizing any environmental or social impacts. If deployed near coastal regions, ocean power plants can supply electricity to these populous regions over a short distance, further reducing transmission costs and losses. Although holding a promising future, ocean wave plants remain a long shot, since wave energy converter (WEC) technologies are still at an early stage and the levelized cost of wave energy is still too high.

One of the most common types of wave energy converters is based on oscillating bodies. It uses floating wave capture bodies (WCB) to extract kinetic energy from ocean waves. These WCBs can take the form of a point absorber (Murai et al., 2021), a terminator (Whittaker et al., 2012) or an attenuator (Henderson, 2006). Different forms have different advantages depending on deployment locations, wave characteristics and energy applications etc. There has not been a convergence as to which form will dominate in the utility scale energy market. But no matter what form it takes, the percentage of capital expenditure on WCBs increases dramatically with the scale of the device (Choupin et al., 2021). Considering that large scale devices are necessary to fully leverage the available wave power, the WCB cost share would dominate the WEC cost and it is important to maximize the generated energy for a given WCB design.

WCB is connected to the electrical loads through power takeoff (PTO) systems, which are a set of mechanical and electrical components that transform the body kinetic energy

to electricity. The design of PTO systems as well as the associated control systems can have a tremendous impact on the actual power output of the WEC. Over the years different types of PTO design are developed and tested to maximize energy outputs. Among them PTO based on hydraulic transmissions is a popular choice due to its robust handling of large loads. There are hydraulic systems that are designed to approach optimal linear control effects with a simple control system (António, 2007). Hydraulic systems can also be easily combined with a phase control strategy called latching control to further boost energy outputs (Liu et al., 2021). Although preferred for large scale WECs, hydraulic PTOs have their shortcomings in terms of high maintenance costs. The oil leakage of hydraulic circuits poses a significant threat to the marine ecology system and the requirements for proper sealing treatment increase the overall costs. Therefore, PTOs involving only mechanical parts are also being investigated.

Depending on the complexity of the mechanical transmissions, there are generally two distinct types of mechanical PTO. One is direct drive PTO, which has a generator move at the same speed as the WCB by eliminating any speed amplification mechanism in between. Specially designed generators are needed to produce electricity efficiently under the low speed high force load profile, such as the linear tubular generator designed by Huang et al. (Huang et al., 2017). The problem with those generators is that their size increases dramatically with the WEC scale. This can create various issues but most importantly can significantly drive up the cost. Instead, another type of mechanical PTO uses speed amplification drivetrain to have the generator working at a higher speed, allowing more compact commercially-available generators to be used. The price to pay here, however, is the increased losses brought by the drivetrain.

It's well known that advanced control can greatly increase the

power output of a given WCB. But in real world, fully realizing the theoretical control benefits is challenging due to various constraints on the PTO and WCB. For example, optimal control typically requires reactive power supplied from the load, and the peak of this reactive power can be much larger than active power (Ringwood, 2020). Then, to fully realize this optimal control needs not only a more complicated PTO that supports bi-directional power flow, but also significantly overrated components. All of these requirements drive up costs and reduce the reliability of the WEC system, offsetting the potential power gains.

Recently, a motion rectification mechanism was invented and integrated into the conventional mechanical drivetrain (Li et al., 2020a). It uses two one-way clutches to rectify the oscillating motion of the WCB, similar to how diodes are used to rectify AC voltage. The primary motivation of this mechanical motion rectifier (MMR) is to keep the generator rotating unidirectionally and use flywheels to maintain the generator's speed. It is found this mechanism can increase power outputs with a simple linear damping control (Li et al., 2020b). This power increase is attributed to a unique disengagement phenomenon where the generator is decoupled from the WCB during parts of the excitation period. However, this disengagement phenomenon is only notable under high frequency excitations, whereas ocean waves tend to concentrate in low frequency ranges.

Since disengagement is the key to power increases. A natural thought is to explicitly control the disengagement. But the disengagement of the MMR PTO depends implicitly on the system dynamics and thus is hard to control. To address this challenge, a new active mechanical motion rectifier (AMMR) is designed (Yang et al., 2021). This AMMR uses controllable electromagnetic clutches in place of the one-way clutches in the MMR, making disengagement fully controllable. However, how to control the clutches to maximize power remains a challenging problem.

In this paper, we present a semi-analytical method to efficiently calculate the harvested mechanical power of a WEC under regular wave excitations. The clutch control is simplified to a scheme of two parameters. A grid of control parameters is swept to find the optimal power region. The resulting optimal control trajectory is analyzed, and the effects of different generator inertia are investigated. The following content is organized with Section 2 describing the WEC system modelling, Section 3 presenting the AMMR control scheme and power calculation method, Section 4 showing the results of the optimal power analysis, and Section 5 concluding the paper.

# 2. WEC MODELLING WITH AMMR PTO

We consider a WEC with a general wave capture body (WCB). The WCB is connected to the generator through a mechanical drivetrain. The AMMR gearbox has two transmission ways to connect the WCB and the generator (Fig. 1). When the positive clutch is engaged, the generator and the WCB move in the same direction. When the negative clutch is engaged, they move in the opposite direction, so that the generator always rotates unidirectionally despite the oscillating motion of the WCB. Moreover, additional inertia such as a flywheel can be

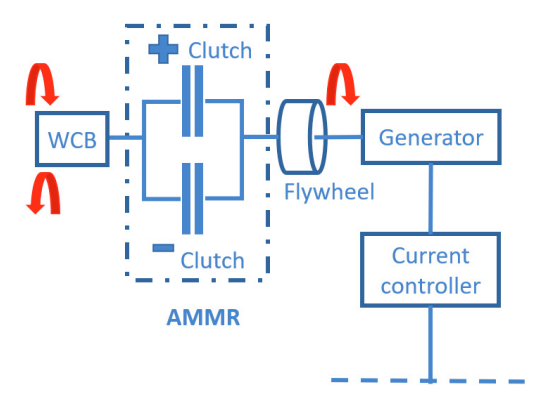


Fig. 1. Simplified model of a WEC with the AMMR PTO

attached to the generator to maintain speed during disengagement phase where both clutches are not engaged. The generator's electromagnetic torque can be controlled by a pulse width modulation (PWM) current controller. The harvested electrical power would be mechanical power input to the generator rotor minus generator and power electronics losses. We neglect these losses and only consider mechanical power in this paper. Consequently, we focus on the mechanical part of the WEC, considering hydrodynamics modelling of wave body interaction and connected PTO dynamics. To capture the essence of the switching dynamics, we consider a WCB constrained to move in one degree of freedom. Then the dynamics equations are constructed in terms of the motion of this WCB. When the generator is engaged, the WCB dynamics is shown in (1):

$$(A(\omega) + m + g^2 m_{pto})\ddot{x} + B(\omega)\dot{x} + Kx = f_{ex}(\omega) + gf_c$$
 (1)

Here we model the WCB hydrodynamics in the frequency domain. With a sinusoidal wave excitation force  $f_{ex}$ , the WCB will have an added mass  $A(\omega)$  and a radiation damping  $B(\omega)$  depending on the excitation frequency  $\omega$ . There are also the body's self-mass m and the mass of the PTO  $m_{pto}$ . Depending on the gear ratio g, the PTO mass can have a quite large impact on the total mass of the system. The hydrostatic buoyance coefficient K is assumed to be constant, which is a good approximation when the displacement x is smaller than 30 degrees. The control force applied through the generator is  $f_c$ . When both clutches are open and the generator is disengaged

. When both clutches are open and the generator is disengaged, the WCB dynamics takes the form of (2):

$$(A(\omega) + m + g^2 m_{n(\alpha)}) \ddot{x} + B(\omega) \dot{x} + Kx = f_{ex}(\omega)$$
 (2)

Here part of the PTO on the generator side of the clutch is decoupled from the WCB, so only the PTO mass on the other side of the clutch  $m_{pto1}$  is lumped into the system mass. During this disengaging phase, the generator can continue rotating and generating energy according to its own dynamics, which is primarily determined by its inertia  $m_{pto2}$  ( $m_{pto1} + m_{pto2} = m_{pto}$ ) and its control force. The system switches between these two dynamics modes according to a control of the clutch status. The control is a sequence of moments specifying when clutches are closed or open. It can have an infinite number of combinations and pose a tremendous challenge for attempts to find an optimal sequence. In the next

section, we will introduce a control scheme that captures the substance of this problem and reduces its dimension to a handleable degree.

## 3. AMMR PTO CONTROL AND POWER

#### 3.1 AMMR PTO Control Scheme

While the AMMR PTO enables us to disengage the generator arbitrarily, there is little justification to disengage more than once for half a wave cycle. Because essentially, disengaging the clutches cuts off the power input to the generator, and from a perspective of maximizing generated power, we only want to do this for good reasons. The first reason to disengage is when the torque transferred by the clutch no longer pushes the generator forward but instead drags it down. This typically happens when the WCB slows down under restoring forces and drags the generator to slow down together. Another reason to disengage is when the WCB can move faster and absorb more power when spinning off the generator. This usually happens when the WCB is rapidly accelerating. In either case, the disengaging needs to happen only once in half a wave cycle since the WCB's motion profile is just accelerating and decelerating for a regular wave excitation.

Based on this rationale, a control scheme for the AMMR PTO is proposed. As shown in Fig. 2, the clutch engagement schedule is defined by two control parameters, engaging phase  $\varphi$  and engaging duration  $t_d$ .  $\varphi$  is a phase shift relative to the sinusoidal excitation. It specifies the time epoch the generator is engaged in a regular wave case. Then,  $t_d$  specifies the time duration it remains engaged before being disengaged. Based on the above argument to disengage at most once in half a wave cycle,  $t_d$  is smaller or equal to  $t_p/2$ , which is half the excitation period. The resulting regular control sequence is an alternating  $t_d$  engagement stage and  $t_p/2-t_d$  disengagement stage. As for the generator torque control during the engagement stage, it makes sense to use a linear velocity feedback control  $f_c = -c_e \omega$  to apply an electric damping torque proportional to the generator velocity  $\omega$ , since the primary objective of the engagement stage is to extract out energy. Linear damping control not only is easy to implement, but also has only one parameter to be optimized, significantly reducing the problem's dimension. With this control scheme, there are three control parameters to be optimized: engaging phase, engaging duration, and damping coefficient.

# 3.2 Power Calculation

The power generation in an AMMR PTO consists of two parts. During the engagement stage, the generator applies a linear damping control, so the generated power is  $c_e \omega^2$ . During the disengagement stage, the generator still can generate energy with its freewheeling effects. Here, it is assumed the kinetic energy stored in the inertia can be fully recovered and control details can be left out. To derive the power generation, an important assumption is the periodicity of the WCB's motion under a regular excitation. Through extensive simulations, it is found the steady state response of the WCB under the proposed control scheme shows a periodic pattern. Fig. 3 shows an example response of an oscillating surge flap. For a

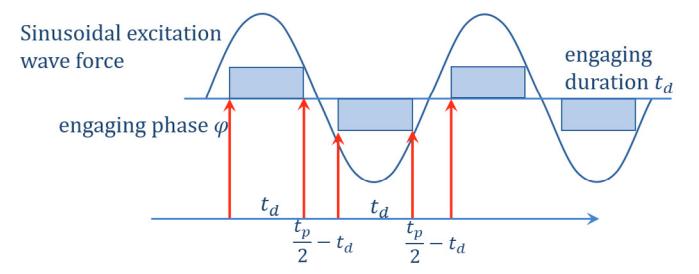


Fig. 2. AMMR clutch control scheme

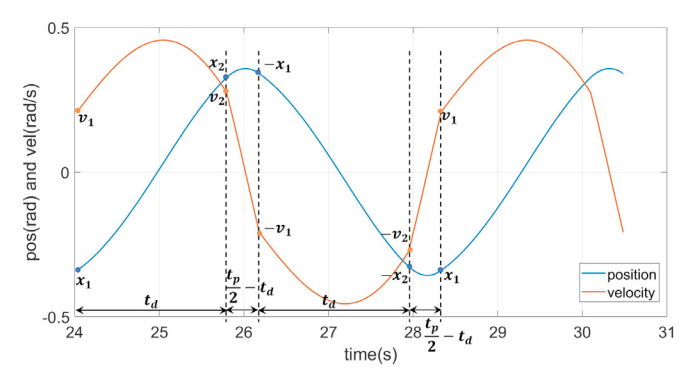


Fig. 3. WCB's periodic response under AMMR control

full cycle, it undergoes four stages of engagement—disengagement—engagement—disengagement. At the moment of the first engagement, its position and velocity is  $(x_1, v_1)$ , then after  $t_d$  time it disengages the generator at a position and velocity of  $(x_2, v_2)$ . After a time of  $t_p / 2 - t_d$ , it reengages the generator at the symmetric position and velocity of  $(-x_1, -v_1)$ . Next, it travels along a mirroring trajectory for the opposite half cycle, disengaging at  $(-x_2, -v_2)$  and reengaging at  $(x_1, v_1)$ .

With this periodicity assumption, we can solve the values of  $(x_1, v_1, x_2, v_2)$  given the control parameters  $(\varphi, t_d, c_e)$ . To see this, we first write the dynamics equations of the WCB in a state-space form. The engagement dynamics (1) can be rewritten as (3):

$$\begin{bmatrix} \dot{x} \\ \dot{v} \end{bmatrix} = \begin{bmatrix} 0 & 1 \\ -K & -K \\ \overline{A(\omega) + m + g^2 m_{pto}} & \frac{-B(\omega) - g^2 c_e}{A(\omega) + m + g^2 m_{pto}} \end{bmatrix} \begin{bmatrix} x \\ v \end{bmatrix} + \begin{bmatrix} 0 & 1 \\ \frac{1}{A(\omega) + m + g^2 m_{pto}} \end{bmatrix} f_{ex}(\omega) \tag{3}$$

Note here we have  $f_c = -c_e gv$ . The disengagement dynamics can be written as (4).

With a sinusoidal excitation  $f_{ex}(\omega) = \Re(F_{ex} * e^{i\omega t})$ , we can explicitly write out the initial value response of a linear dynamic system. Specifically, for a linear system under a harmonic excitation expressed in state space form

 $\dot{X}=AX+\Re(Be^{i(\omega t+\varphi)})$  , the state trajectory from initial value  $X_0$  has close form solution (5).

$$\begin{bmatrix} \dot{x} \\ \dot{v} \end{bmatrix} = \begin{bmatrix} 0 & 1 \\ -K & -B(\omega) \\ \hline A(\omega) + m + g^2 m_{pto1} & A(\omega) + m + g^2 m_{pto1} \end{bmatrix} \begin{bmatrix} x \\ v \end{bmatrix} + \begin{bmatrix} 0 & 1 \\ 1 & A(\omega) + m + g^2 m \\ \hline A(\omega) + m + g^2 m & A(\omega) \end{bmatrix} f_{ex}(\omega)$$
(4)

$$X(t) = e^{A(t-t_0)} X_0$$
  
+\mathfrak{H}(\left( Ie^{i\omega(t-t\_0)} - e^{A(t-t\_0)} \right) \* \left( i\omega I - A \right)^{-1} Be^{i(\omega t\_0 + \phi)} \right) (5)

Then define (x, v) to be X. Equation (3) can be rewritten as:

$$\dot{X} = A_1 X + \Re(B_1 e^{i(\omega t + \varphi)}) \tag{6}$$

And (4) can be rewritten as:

$$\dot{X} = A_2 X + \Re(B_2 e^{i(\omega t + \varphi)}) \tag{7}$$

Next define  $(x_1, v_1)$  to be  $X_1$ ,  $(x_2, v_2)$  to be  $X_2$ . Two sets of equations (8) and (9) can be constructed based on the state transition from  $X_1$  to  $X_2$  and from  $X_2$  to  $-X_1$ :

$$X_{2} = e^{A_{1}t_{d}} X_{1} + \Re((Ie^{i\omega t_{d}} - e^{A_{1}t_{d}}) * (i\omega I - A_{1})^{-1} B_{1}e^{i(\varphi - \pi/2)})$$
(8)

$$-X_{1} = e^{A_{2}(t_{p}/2 - t_{d})} X_{2} + \Re((Ie^{i\omega(t_{p}/2 - t_{d})} - e^{A_{2}(t_{p}/2 - t_{d})})$$

$$*(i\omega I - A_{2})^{-1} B_{2} e^{i(\varphi + \omega t_{d} - \pi/2)})$$
(9)

Combining (8) and (9) provides four independent equations and thus the four unknown variables  $(x_1, v_1, x_2, v_2)$  can be solved. Then the generated energy during the  $t_d$  engagement time is  $\int_0^{t_d} g^2 c_e v^2(t) dt$  with  $v(0) = v_1$ . The value of v(t) can be calculated using (8). The generated energy during the  $t_p/2-t_d$  disengagement time is expressed as the kinetic energy difference  $m_{pto2}(v_2^2-v_1^2)/2$ . If this difference is negative, that means the generator needs to act as a motor to increase speed during the disengagement stage. Finally, the generated power is expressed as the total generated energy for one wave cycle divided by the wave period as:

$$P_{gen} = \left(2 * \int_0^{t_d} g^2 c_e v^2(t) dt + m_{pto2} (v_2^2 - v_1^2)\right) / t_p .$$

#### 4. A SURGE FLAP CASE STUDY

To examine the effectiveness of proposed power calculation method and to find the optimal control values for the proposed control scheme, a surge flap type **WCB** is selected here for a case study. The geometry of the

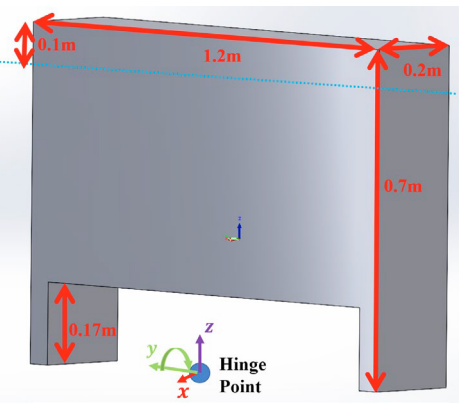


Fig. 4. A surge flap type of WCB investigated

surge flap is shown in Fig. 4. It is hinged at the bottom and constrained to only rotate around the y axis. The wave propagation is along the x axis right against the flap. A prototype of this surge flap was built and tested in a wave tank. The PTO connected to this flap includes a belt drivetrain and the AMMR gearbox. A system identification was performed to estimate the frequency response of the flap and the PTO. An admittance model is estimated at the shaft of the PTO before the clutches. The high order admittance model is then approximated using a spring mass damper model with frequency dependent mass and damping values and a constant stiffness value. Table 1 shows the respective inertia, damping and excitation values of the seven wave periods investigated later. The excitation values are calculated using Nemol based on 0.1m wave amplitude.

Table 1. WEC model parameters

Wave	Inertia(Kg.m <sup>2</sup> )	Damping	Excitation
period(s)		(Nms/rad)	(Nm/0.1m)
1.7	87	186	260
2.4	77	75	129
2.7	73	63	106
3	68	57	91
3.6	60	55	72
4.3	50	61	58
5	41	71	49

The hydrostatic stiffness of the flap is measured to be 285 Nm/rad. The inertia of the AMMR gearbox before the clutches  $(m_{pto1})$  is measured to be 0.0001 Kg.m², while the inertia after the clutches including the generator inertia ( $m_{pto2}$ ) is measured to be 0.00008 Kg.m². The combined gear ratio g of the belt and gear drivetrains is 395.

# 4.1 Optimal Power

Although the semi-analytical method presented in section 3.2 significantly shortens the time required to get the steady state power given control parameters  $(\varphi,t_d,c_e)$ , it still takes subsecond level time for a single evaluation, making it too time-consuming to apply a numerical optimization solver. Instead, a mesh grid of points are evaluated to find the optimal power point. In this study, a  $10\times15\times100$  mesh is used, with  $\varphi$  taking values from  $0.09\pi$ ,  $t_d$  taking values from  $0.2\pi/\omega$  to  $0.5\pi/\omega$ ,

and  $c_e$  taking values from 0.0001 Nms/rad to 0.01 Nms/rad. Moreover, from a control co-design perspective, optimal power is found for 10 different levels of generator inertia  $m_{pto2}$  to evaluate its influences on power. The results are compared to a base system with a normal mechanical PTO under a linear damping control, which has a close form optimal power solution (11) (Falnes and Kurniawan, 2020).

$$\frac{F_{ex}^{2}(\omega)/4}{B(\omega)+\sqrt{\left(B^{2}(\omega)+(\omega(A(\omega)+m+g^{2}m_{pto})-K/\omega)^{2}\right)}}$$
(11)

The results are shown in Fig. 5. Since for the selected surge flap the excitation force amplitude decreases as wave period gets longer, the generated power also drops monotonically with the wave periods. The flap was designed to resonate with 3 second wave, but with PTO connected the resonance peak

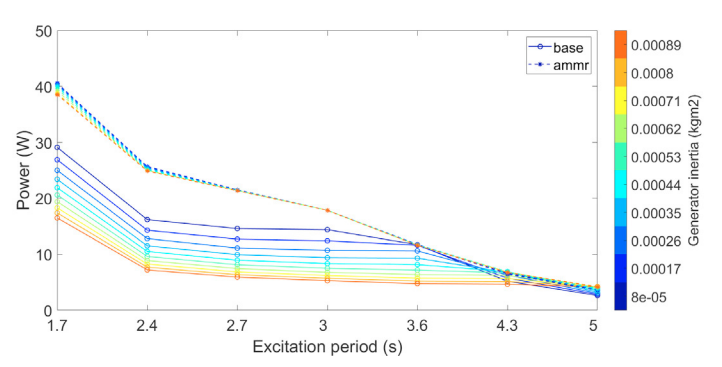
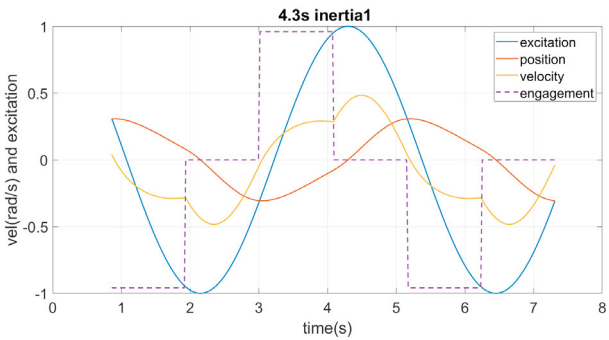


Fig. 5. Optimal power of AMMR and base PTO

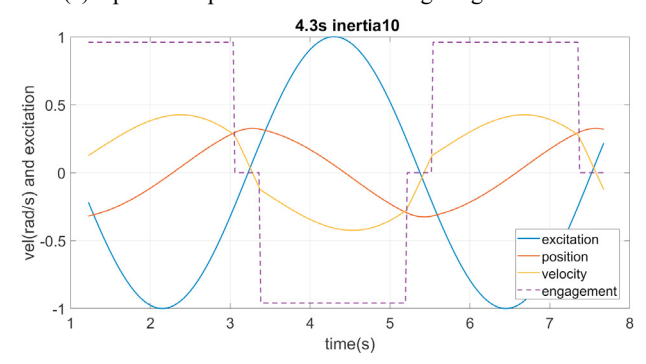
disappears due to excessive damping brought by the PTO drivetrain. From the results, an important observation is that generator inertia has quite different influences on the optimal generated power between a normal mechanical PTO and an AMMR PTO. For a normal PTO, different generator inertia values influence the optimal power at different wave periods. But for an AMMR PTO, there is no such influence. Considering that at each single frequency, the WEC system is modelled as a spring mass damper system, varying generator inertia essentially changes the system's natural frequency, which determines its power generation at different wave periods. However, with AMMR control, natural frequency is no longer important, as the clutch disengagement control can always compensate for any mismatches of the frequency.

# 4.2 Optimal Control Response

By examining the response of the flap motion under the optimal control, it can be found that the AMMR control improves power by aligning the velocity of the flap in phase with the excitation force. The flap trajectories under three wave periods, which are higher, equal or lower than the flap's natural period, are plotted in Fig. 6–8. Only the phase is shown in the figures for the sinusoidal excitation force (amplitude is scaled to 1). It can be seen that for all four cases in Fig. 7 and 8, the engagement stage starts when the excitation is waning, and at the time of the engagement the flap is at its highest speed after a rapid acceleration during the disengagement stage. While for longer wave periods shown in Fig. 6, the flap engages at low speed when the excitation starts to soar. The reason behind the optimal control shown in Fig. 7 and 8 is

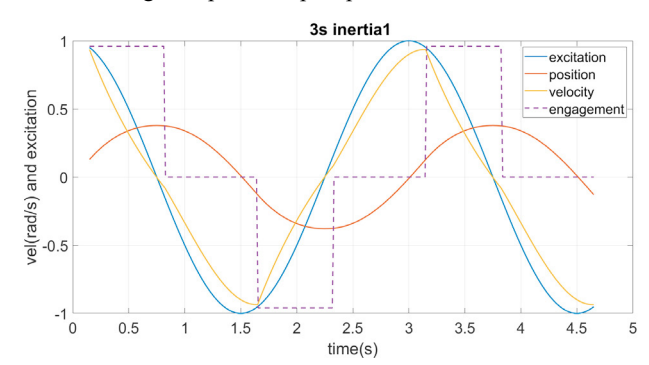


(a) Optimal response with 0.00008 Kg.m<sup>2</sup> generator inertia

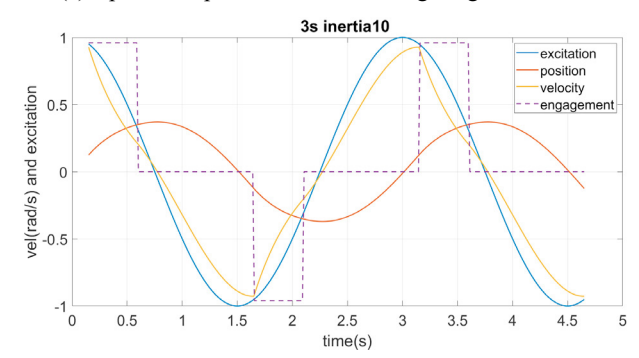


(b) Optimal response with 0.00089 Kg.m² generator inertia

Fig. 6. Optimal flap response under 4.3 s wave



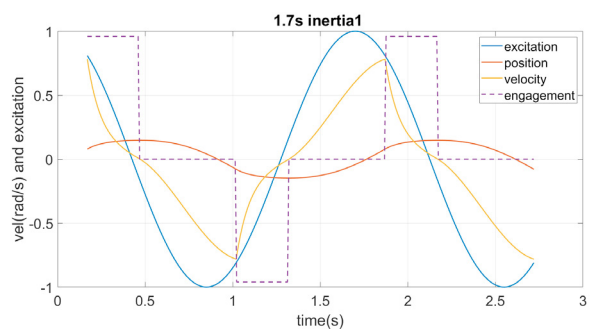
(a) Optimal response with 0.00008 Kg.m<sup>2</sup> generator inertia



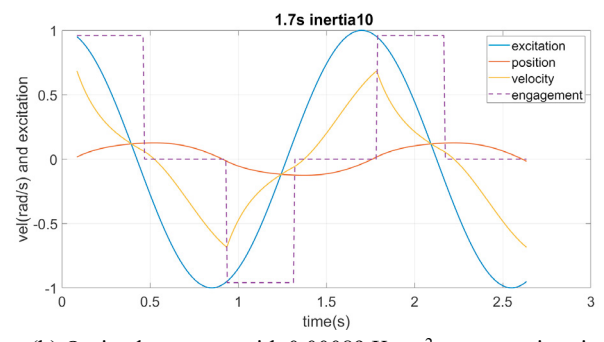
(b) Optimal response with 0.00089 Kg.m<sup>2</sup> generator inertia

Fig. 7. Optimal flap response under 3 s wave

twofold. First, in all four cases the WEC has a lower natural frequency than the excitation frequency, which typically leads to phase lags of the velocity. The control compensates the phase lag by spinning off the generator load during excitation soaring and dragging down the speed during excitation waning. Second, the excitation magnitude is strong enough to bring the flap to a sufficiently high speed during the disengagement



(a) Optimal response with 0.00008 Kg.m<sup>2</sup> generator inertia



(b) Optimal response with 0.00089 Kg.m<sup>2</sup> generator inertia Fig. 8. Optimal flap response under 1.7 s wave

stage, storing enough energy for the generator to absorb during the excitation waning. The reason behind the optimal control shown in Fig. 6 is subtler. The case in Fig. 6 (b) also has a lower natural frequency, but it doesn't show similar control profile as Fig. 7 and 8. It's because the excitation amplitude is low at 4.3s wave, thus not able to drive the flap to a high speed. Instead, it compensates the phase lag by disengaging when the generator is dragged down by the flap, allowing the flap to decelerate faster. The case in Fig. 6 (a) has a higher natural frequency than the wave and the velocity would have a phase lead. The optimal control disengages the generator early before the excitation reaches its peak. This gives the flap the chance to move further against the restoring stiffness force, essentially delaying its reversing time and compensating for the phase lead. By analyzing the rationale behind the found optimal control, practical methods can be constructed for controlling the AMMR PTO in real world wave scenarios.

# 5. CONCLUSIONS

In this paper, an efficient computational method is introduced to evaluate the optimal power potential of a newly developed AMMR PTO, which aims at increasing WEC power outputs across a wide wave spectrum. A case study with a surge flap type of wave capture body shows the developed method is numerically stable and fast enough to evaluate a fine mesh grid of control parameters. The obtained optimal power for the case study confirms the hypothesis of the AMMR PTO's broadband superiority. Detailed analysis of the found optimal control trajectories reveals how the disengagement mechanism is used to align the velocity of the flap in phase with the excitation force to maximize the power. These findings provide useful guidance as to designing practical control algorithms for operating under real world waves.

### ACKNOWLEDGEMENT

This research is supported by the funding provided through the DOE grant E-EE0008953, DOE seeding grant DE-NA0003525, and NSF IUCRC 1738689.

#### REFERENCES

- António, F.D.O., 2007. Modelling and control of oscillating-body wave energy converters with hydraulic power take-off and gas accumulator. *Ocean engineering*, 34(14-15), pp.2021-2032.
- Choupin, O., Henriksen, M., Etemad-Shahidi, A. and Tomlinson, R., 2021. Breaking-down and parameterising wave energy converter costs using the CapEx and similitude methods. *Energies*, 14(4), p.902.
- Falnes, J. and Kurniawan, A., 2020. Ocean waves and oscillating systems: linear interactions including wave-energy extraction (Vol. 8). Cambridge university press.
- Henderson, R., 2006. Design, simulation, and testing of a novel hydraulic power take-off system for the Pelamis wave energy converter. *Renewable energy*, 31(2), pp.271-283
- Huang, L., Hu, M., Chen, Z., Yu, H. and Liu, C., 2017. Research on a direct-drive wave energy converter using an outer-PM linear tubular generator. *IEEE Transactions on Magnetics*, 53(6), pp.1-4.
- Lehmann, M., Karimpour, F., Goudey, C.A., Jacobson, P.T. and Alam, M.R., 2017. Ocean wave energy in the United States: Current status and future perspectives. *Renewable and Sustainable Energy Reviews*, 74, pp.1300-1313.
- Li, X., Chen, C., Li, Q., Xu, L., Liang, C., Ngo, K., Parker, R.G. and Zuo, L., 2020. A compact mechanical power take-off for wave energy converters: Design, analysis, and test verification. *Applied Energy*, 278, p.115459.
- Li, X., Liang, C., Chen, C.A., Xiong, Q., Parker, R.G. and Zuo, L., 2020. Optimum power analysis of a self-reactive wave energy point absorber with mechanically-driven power take-offs. *Energy*, 195, p.116927.
- Liu, C., Hu, M., Zhao, Z., Zeng, Y., Gao, W., Chen, J., Yan, H., Zhang, J., Yang, Q., Bao, G. and Chen, S., 2021. Latching control of a raft-type wave energy converter with a hydraulic power take-off system. *Ocean Engineering*, 236, p.109512.
- Murai, M., Li, Q. and Funada, J., 2021. Study on power generation of single Point Absorber Wave Energy Converters (PA-WECs) and arrays of PA-WECs. *Renewable Energy*, 164, pp.1121-1132.
- Ringwood, J.V., 2020. Wave energy control: status and perspectives 2020. IFAC-PapersOnLine, 53(2), pp.12271-12282.Scruggs, J. and Jacob, P., 2009. Harvesting ocean wave energy. Science, 323(5918), pp.1176-1178.
- Whittaker, T. and Folley, M., 2012. Nearshore oscillating wave surge converters and the development of Oyster. *Philosophical Transactions of the Royal Society A: Mathematical, Physical and Engineering Sciences*, 370(1959), pp.345-364.
- Yang, L., Huang, J., Congpuong, N., Chen, S., Mi, J., Bacelli, G. and Zuo, L., 2021. Control Co-design and Characterization of a Power Takeoff for Wave Energy Conversion based on Active Mechanical Motion Rectification. *IFAC-PapersOnLine*, 54(20), pp.198-203.